Numerical investigation of the refraction effects by jet flows in anechoic wind tunnels

Stéphane REDONNET[1]; Jean BULTE[2]

[1,2] ONERA (French Aerospace Centre), France

ABSTRACT

In regard to the problem of aircraft noise mitigation, the present study focuses on the refraction effects to be possibly induced by anechoic facility jet flows on the measured acoustic signatures, during typical airframe noise experiments. To this end, Computational AeroAcoustics (CAA) calculations based on the solving of the Perturbed Euler Equations (PEE) are conducted, enabling the estimation of the refraction effects characterizing a typical open-jet, anechoic wind tunnel, namely the NASA Langley's Quiet Flow Facility (QFF). Coming along with their validation against analytical results obtained through a Ray Tracing (RT) technique, the analysis of these CAA/PEE calculations highlights the refraction effects by the facility jet flow, delivering preliminary insights about what are the key parameters (jet height, jet curvature, jet spreading angle, shear layer thickness, etc.) to play a major role in these refraction phenomena.

Keywords: Aircraft Noise Mitigation, Facility Installation Effects, Refraction Effects I-INCE Classification of Subjects Number(s): 23.2; 73.1; 76.9
(See . http://www.inceusa.org/links/Subj%20Class%20-%20Formatted.pdf .)

1. INTRODUCTION

A few years ago, noise annoyances by aircraft were officially identified as the major obstacle to a sustainable growth of air traffic. Therefore, all stakeholders involved in the development of aircraft systems or components now focus on practical ways to reduce the acoustic signature by their products. On another hand, since acoustics is a complex discipline, they are often bounded to make an intensive use of numerical simulations, which constitutes a powerful R&D tool, when used in complement to experimentation. In particular, a synergy must be established between the computational and the experimental worlds, so that each benefit from the other; indeed, whereas it is mandatory that the various numerical techniques are validated through reliable experiments, it is also highly desirable that the latter testing procedures and environments take direct benefit from the additional information offered by computational means, which can improve the relevance and the confidence in the experimental measurements acquired.

This is the reason why, recently, dedicated studies were jointly conducted by Onera and NASA (1, 2), so as to numerically assess the acoustic installation effects that may occur in the Quiet Flow Facility (QFF) of NASA Langley Research Center (LaRC). Consisting in numerical simulations relying on a Computational AeroAcoustics (CAA) approach, these studies made it possible, first, to evaluate and, then, to discriminate the diverse acoustic installation effects to be possibly induced by the facility components (e.g., mounting side plates, nozzle, collector plate) or features (e.g., confined jet vs. co-flow) onto airframe noise experiments that are usually conducted within QFF (3-6). At the light of these studies, it appeared that, although they were rather modest compared to the reflection / diffraction effects inherited from the experimental apparatus, the refraction effects resulting from the facility jet flow might impact the noise propagation in a non-negligible way, for instance by altering importantly the acoustic phase – a thing that could question the application of array localization techniques within facility environments (7).

[1] Stephane.Redonnet@Onera.fr
[2] Jean.Bulte@Onera.fr

Therefore, follow-on computations were recently achieved on the basis of these previous works, with the view of investigating more closely the sole refraction effects to be expected from the jet flow of typical anechoic facilities such as NASA's LaRC QFF. The aim of such study, which constitutes the purpose of the present paper, was twofold; first objective was to assess how similar the refraction effects by a QFF-like jet flow (*e.g.*, 3D jet with spreading shear layers, etc) could be, compared the ones induced by more idealized configurations (co-planar jet with an infinitely thin shear layer, etc.) on which generally rely the analytical corrections (8) that are commonly applied to experimental data for de-biasing them from refraction effects - such as commonly done in QFF tests. Second objective of the study was to perform a preliminary assessment of what might be the key parameters (jet height and/or curvature, shear layer thickness and/or spreading angle, etc.) to play a more prominent role in such jet flow refraction effects.

2. COMPUTATIONAL APPROACH

2.1 Computational Strategy

For numerically investigating the acoustic installation effects that may occur within facility environments due to the experimental set up and/or jet flow, one can preferably make use of an advanced acoustic hybrid approach (9) involving a noise propagation stage based on the Perturbed Euler Equations (PEE). Indeed, one can here recall that only a Computational AeroAcoustics (CAA) technique[1] relying on the PEE (10-13) or a linearized version thereof can simultaneously account for i) the reflection/diffraction effects by the solid devices of the experimental apparatus and ii) the refraction effects by the flow heterogeneities of the facility jet, in contrast to other techniques that can only model the former - such as the Boundary Element Method, or even neither of them - such as Integral Methods (14-16).

Although one can advantageously weak-couple such CAA-based noise propagation stage with a CFD-based sound generation one[2] (1, 17, 18), in some cases, it may be sufficient to consider it alone, i.e. to perform pure CAA calculations based on simplistic sources - this enabling interesting qualitative studies to be achieved at a much more reasonable cost (9). This only requires that enough information is known about the noise generation stage for equivalent sources are analytically synthesized, based on the characteristics (location, frequency, relative magnitude, etc.) of the acoustic emission. On that stage, one can recall that airframe noise sources (which are solely sought after, in QFF experiments) can generally be decomposed into either monopoles (e.g., thickness noise) or dipoles (e.g., loading noise) emitting at a given tonal frequency. Additionally, any dipole can be further decomposed as a sum of two monopoles (located each one nearby the other, but pulsating in phase opposition).

Therefore, in the present case, the numerical strategy consisted in performing CAA/PEE computations alone, with all these calculations involving an identical equivalent source based on a (multi)tonal monopole. On another hand, these simulations were allotted various background mean flows (see section 2.2, below), which were chosen so that a certain number of specific canonical situations are addressed, and the key parameters underlying their respective refraction effects are highlighted. Finally, since only refraction effects were sought at here, and contrarily to what had been done in the previous works (1, 2), none of the QFF set-up devices was incorporated to the calculations; the propagation medium was thus considered as a free field, as implicitly assumed in the analytical corrections (8), which are, at best, based on a round or a parallel *isolated* jet flow.

As a validation step, the CAA/PEE simulations associated with the more meaningful configurations were compared against analytical calculations relying on a Ray Tracing (RT) approach. Being based on works achieved by Candel in the late 70's and implying solely a high frequency approximation (that is, here, assuming a source which wavelength is small enough compared to the jet shear layer thickness), the latter approach can accurately account for the refraction effects by any jet mean flow, whether its characteristics are.

2.2 Computational Means

All CAA calculations were performed with the help of ONERA's *sAbrinA* solver (Redonnet et al, since 2000), which is a structured, time-accurate CAA code that solves either the full or the linear Euler

[1] Whether it is based on high-order finite-difference (FD) schemes operating on multi-block structured grids, or on the so-called Discontinuous Galerkin Method, which is based on unstructured grids.

[2] Such as previously done by the present first author for numerically assessing the acoustic installation effects by anechoic facility environments onto various airframe noise emissions (1, 18).

equations, in a conservative and perturbed form. The solver employs finite-difference operators, involving high-order spatial derivatives and filters, as well as a 3rd-order, multi-stage, Runge-Kutta time-marching scheme. The code deals with multi-block structured grids with one-to-one interfaces, and is fully parallelized using the Message Passing Interface (MPI) standard. Finally, the solver includes the usual boundary conditions (reflection by solid walls, non-reflecting / free-field radiation, etc.), as well as some unique to specific applications. More detailed information about *sAbrinA* solver and its underlying methodology can be found in Refs. 10-13.

All Ray Tracing calculations were achieved with the help of ONERA's *MadMax* code (Bulte, 2014), which is an integrated suite of Matlab modules that allow performing analytical predictions of acoustic propagation in a fast and accurate manner.

3. COMPUTATIONAL SET-UP

3.1 Mean Flow

As said above, several types of background mean flow were considered, so as to allow the proper assessment of all various flow effects, while staying close enough from the QFF experimental conditions; for all configurations, the background pressure field was taken as homogeneous, with a nominal value corresponding to the atmospheric conditions (P_o = 101325 *Pa*). In contrast, the background velocity and density fields were taken as possibly heterogeneous, depending on the case. First, the velocity field was prescribed a generic jet profile, which was derived with the help of similarity functions based on a given set of parameters. More precisely, such velocity profile was driven by both i) the Mach ratio M_r between Mach numbers in the jet core and at infinity ($M_r = M_\infty/M_{core}$) and by ii) the spreading angle (α) of the jet's mixing layers (see Figure 1). On another hand, the density field was derived via the Crocco-Buseman relation, which relates the local temperature to the velocity. Such density field was thus not only driven by the Mach ratio (M_r), but also by the temperature ratio T_r between the temperature in the jet core and at infinity ($T_r = T_\infty/T_{core}$). With the view of covering enough canonical situations as well as of easing a systematic assessment of their associated refraction effects, these Mach and temperature ratios were allotted different values, depending on if the medium was to be considered as a uniform flow (M_r = 1) or a sheared jet (M_r = 0), to be taken as adiabatic (T_r = 1) or not ($T_r \neq 1$), and to be allotted a spreading angle ($\alpha \neq 0$) or not ($\alpha = 0$). On the same way, for matching the academic configurations (and, thus, usual corrections) that are classically provided in the literature, both 2D and 3D-axisymmetric jet configurations were addressed.

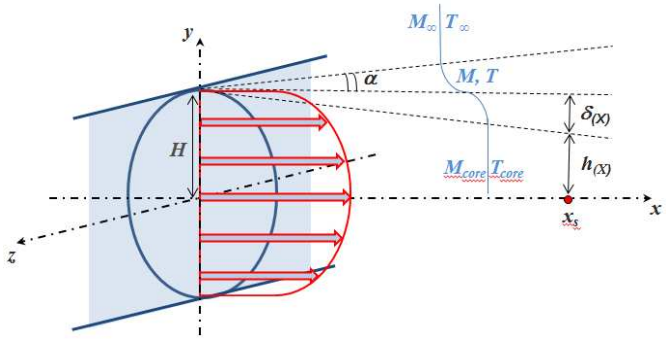

Figure 1 – Sketch of the jet flows (2D or 3D-axi), with associated parameters

Table 1 – Configurations investigated and characteristics of associated background mean flows

Configuration	Background Mean Flow	M_r	α	T_r
A	Uniform	1	-	1
B	2D parallel jet (thin shear layers)	0	0°	1
C	2D parallel jet (thick shear layers)	0	0°	1
D	2D spreaded jet (thick shear layers)	0	7°	0.937
E	3D-axi parallel jet (thin shear layers)	0	0°	1
F	3D-axi spreaded jet (thick shear layers)	0	7°	0.937

For all calculations, the flow parameters were adjusted to the nominal values usually recorded within the QFF; in particular, the jet core Mach number was chosen as $M_{core} = 0.17$, whereas the temperature at infinity T_∞ was set to 293*K* (i.e. 67°F). In the same way, when applicable, the velocity profile's boundary layer thickness was allotted a representative value of 0.6". All other parameters were derived from these ones, depending on the configuration chosen; a first calculation (configuration A) involved a uniform flow ($M_r = 1$, $T_r = 1$), so as to deliver a reference solution (e.g. free of any refraction effect). On the contrary, five additional calculations (configurations B to F) involved a heterogeneous mean flow, each one corresponding to a particular sheared configuration ($M_r = 0$); the three first ones (configurations B, C, D) incorporated a *parallel jet* (*i.e.,* 2D), for which the boundary layer thickness, the spreading angle and/or the temperature ratio were varied (see Table 1). The two remaining calculations (configurations E, F) focused on the *round jet* (*i.e.,* 3D-axi) version of the parallel flow addressed in configurations B and D. Table 1 details the parameters associated with these various configurations.

3.2 Acoustic Source

As said above, and following what had been done in the previous works (2), all CAA computations were based on an equivalent source, which was composed of a *multi-tonal* monopole; more precisely, the source point was defined as a sum of 8 monopoles, each one being allotted an arbitrary amplitude, as well as a particular frequency corresponding to a multiple of a given fundamental one. The latter fundamental frequency was set to $f_1 = 1.115$ *kHz* so that its associated wavelength[1] equals $\lambda_1 = H$ (with *H* the half-height of the test section[2]). Each one of the 7 other tones (source's harmonics) had a frequency given by $f_n = n \times f_1$, with *n* the number of tones considered (i.e. $f_{2,3,\ldots,8} = 2.23$ *kHz*,…, 8.92 *kHz*), that is, was associated with a wavelength of $\lambda_n = H/n$ (i.e. $\lambda_{2,3,\ldots,8} = H/2,\ldots, H/8$). On this stage, one can precise that privileging moderate to high frequencies sources was made on purpose, in order to examine the relative weight that refraction effects may have onto acoustic waves of small wavelengths / high frequencies, which are often of more relevance to small-scale wind tunnel testing. Indeed, in the present case, the upper harmonic source (8th tone) exhibited a frequency of almost 9*kHz*, a value that is not far away from the 10*kHz* upper limit beyond which, for the present flow configuration, other phenomena may arise (which cannot be easily simulated via CAA/PEE, e.g. diffusion by small scale turbulence). Additionally, one can also precise that specifying these multi-tonal sources as pure harmonics of a fundamental one was also made on purpose, in order to enable simulating them in one shot, via a single time domain CAA calculation (to be post-processed through Fourier transforms in time, delivering then each source respective contribution to the overall radiation field). Finally, such equivalent (multi-tonal monopolar) source was located downstream the jet axis, at a distance of 3.5*H* (*i.e.,* 42") from the nozzle exit - a location that is representative of what may be encountered in airframe noise experiments conducted in QFF (where models are usually positioned at a location that ranges from 2*H* to 4*H*).

Here it is worth mentioning that, in canonical situations such as the present ones (configurations B to F), the acoustic refraction is expected to be primarily driven by the aspect ratio between the source wavelength and the jet's shear layer (half) thickness $\delta_{(x)}$ or (half) height $h_{(x)}$ (with $h_{(x)} = H - \delta_{(x)}$, where *H* defines the half height of the nozzle section exit). The latter can be expressed under the form of two non-dimensionalized parameters γ and β, respectively given by $\gamma_{(x,f)} = \delta_{(x)}/\lambda$ and $\beta_{(x,f)} = h_{(x)}/\lambda$.

Table 2 – Non-dimenzionalized parameters characterizing the jet-to-source key aspect ratio (n = 1, 2, 3, … 8)

Configuration	$\gamma_n = \delta(x_s)/\lambda_n$	$\beta_n = h(x_s)/\lambda_n$
B	0	n
C	$0.05 \times n$	$0.95 \times n$
D	$0.4797 \times n$	$0.52025 \times n$
E	0	n
F	$0.4797 \times n$	$0.52025 \times n$

[1] Within the *yz* plane, i.e. free of any Doppler effect.
[2] One can here recall that QFF nozzle is of rectangular shape, and of dimensions $3H \times 2H$, with $H = 12$".

With respect to the acoustic source location (x_S = 3.5H) and various wavelengths ($\lambda_{n=1,\ldots,8}$ = H/n) considered here, Table 2 provides the values taken by these two parameters for each configuration B to F; as one can see, parameter γ ranked from 0 (for both configurations B and E, at all frequencies) to 3.8376 (for both configurations D and F, at the higher frequency), whereas its counterpart β ranked from 0.520025 to 4.162 (for both configurations D and F, depending on the frequency).

3.3 CAA Mesh

In order to save computational resources, benefit was taken from the double symmetry offered by all configurations with respect to the *xy* and *xz* planes. Therefore, only one quarter of the domain was meshed, which was achieved thanks to a unique CAA grid. The latter was generated following precise meshing criteria, which were driven by the dual need of i) a sufficient discretization of acoustic waves (especially those of higher frequency, e.g. f_8 tone) all over the domain and ii) a decent mesh resolution within the jet shear layers areas, whenever needed. In particular, an automatic grid refinement (based on the Malesh transform) was applied over the sheared flow region, ensuring that at least 12 to 15 grid points were present in the mixing layers (especially regarding the configuration C, for which the parallel mixing layers' thickness was of 0.6" i.e. H/20).

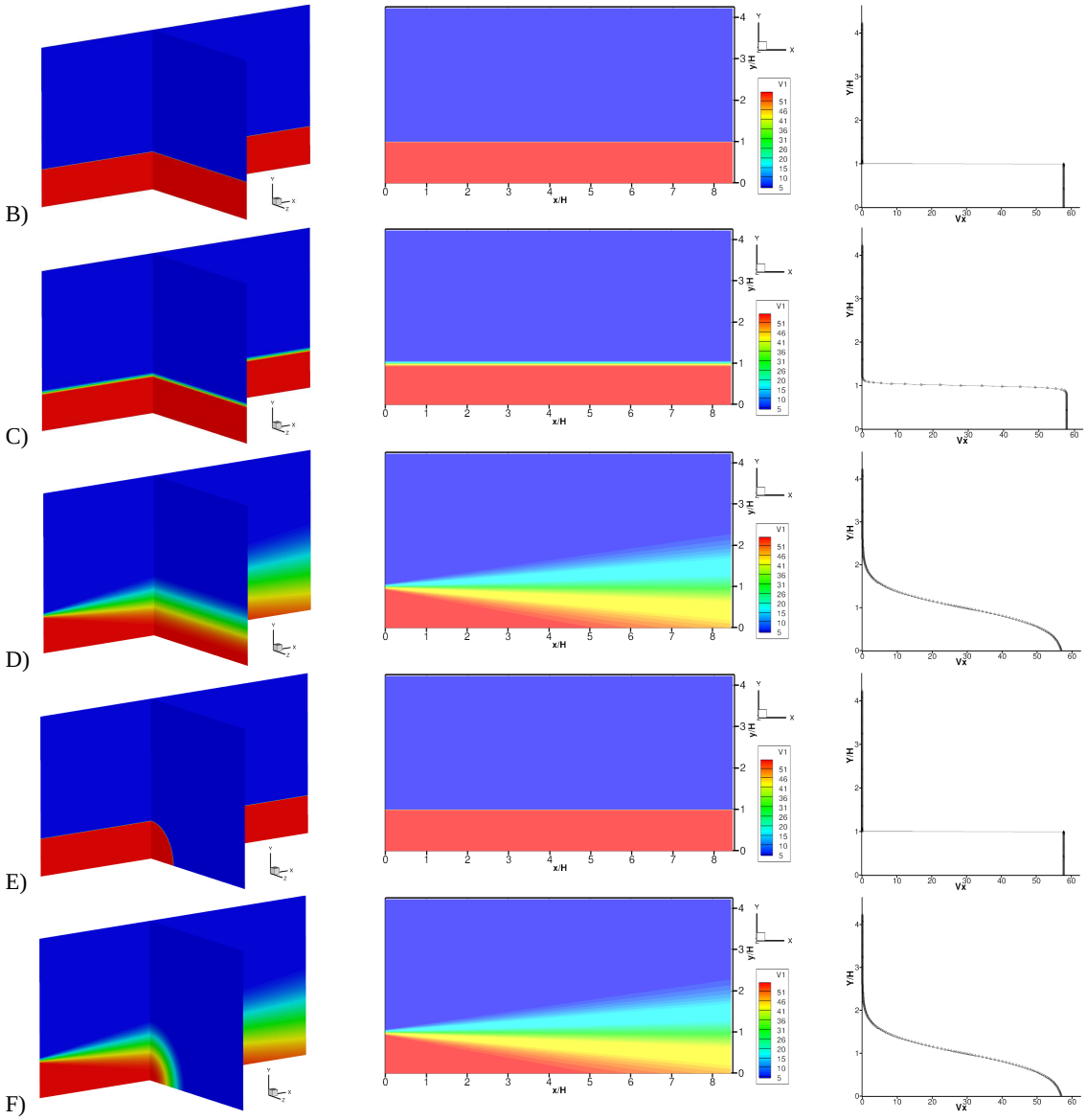

Figure 2 – Background mean flow associated with configurations B to F (from top to bottom, respectively). Axial velocity field (in *m*/*s*) within the *xy* and/or *yz* half-planes (left and middle) or along the *y*-line (right) passing by the source. On right side, the symbols denote the CAA grid points in the *y*-direction

This resulted in a heterogeneous Cartesian monoblock of $482 \times 211 \times 205$ (i.e. approx. 21.3 millions) points[1], which extended up to a distance of 100" (i.e. 8.5*H*) in the jet axis and 50" (4.25*H*) in the two lateral directions. As an illustration, Figure 2 plots the background mean flows that were derived onto the CAA mesh with respect to configurations B to F. In this figure, one can appreciate how, whenever needed, the boundary / mixing layers were sufficiently discretized, thanks to the local clustering of the mesh.

Once such grid + flow inputs were processed for parallel computing, the CAA calculations were run over 468 cores of Onera's super computer. Each simulation was run until a stationary state has established all over the computational domain, which required a physical duration of 8 (resp. 64) times the period associated with the fundamental (resp. 8th) tone emitted. The time step used in the simulations was such that the corresponding temporal discretization was of 200 (resp. 25) iterations per period. Thanks to the number of cores used, each CAA calculation (of 21 million of grid points / 1600 iterations) was completed in less than 2 hours of wall-clock time.

4. RESULTS AND ANALYSIS

Thanks to the numerous configurations that were implicitly addressed here (6 flow conditions, 8 frequencies, 2 prediction approaches, etc.), a large amount of results were acquired, and analyzed (at the present date, the analysis is still going on). For consistency's sake, only a fraction of the outcomes that were gathered so far are presented here. In particular, only the results associated with the higher frequency case (f_8) are shown and briefly discussed below. The remaining part of all results acquired and analyses conducted will constitute the matter of a more extensive communication, to be given in a near future (20).

4.1 Radiation of the High Frequency Source within the Various Jet Flows

Figure 3 displays three planar views of the instantaneous perturbed pressure field associated with the source of higher frequency (f_8), as obtained at the end of each CAA/PEE calculation. As one can see, compared to the uniform flow case (configuration A), the acoustic radiation is more or less importantly altered by the jet flow, depending on the case. In particular, for all configurations B to F, and despite of the fact they were initially emitted in a pure isotropic fashion, acoustic waves propagate in a very anisotropic manner within the *xy* plane – which obviously comes from the refraction effects by the jet shear layers. As a result of that, the acoustic fields exhibit a rather directive signature, especially upstream and downstream the source location. In particular, one can notice the strong interaction patterns that acoustic waves exhibit over these regions, which translate backscattering effects by the shear layers. This is coherent with what can be predicted analytically and observed experimentally, with shear layers that scatter back towards the jet axis region those grazing acoustic waves which angle of incidence is lower than a limit angle. At this stage, one can notice how all these effects appear to be more prominent when the jet is not spreading (configurations B, C and E) and, in a lesser extent, when it is curved (compare for instance configurations E and F to configurations B and D, respectively). One can also notice how, when shear layers do not spread out, their thickness does not seem to play a significant role in these refraction effects (compare for instance configurations B and C), which indirectly confirms the validity of the infinitely thin shear layer assumption on which analytical (*e.g.*, Amiet) corrections generally rely.

The impact that such refraction effects by flow heterogeneities may have onto the radiated acoustic energy appear more clearly in Figure 4, which displays the Root Mean Square (RMS) of the perturbed pressure fields obtained within the $z = 0$ half-plane. Here again, the effect of the various shear profiles are clearly visible, whether it is in terms of modified directivity, or in terms of energy confinement in the upstream and downstream part of the domain. And here again, one can notice that, these effects appear to be less pronounced when the jet flow is realistic (*e.g.*, spreading – see configurations D and F) than when it corresponds to a more idealized situations (configurations B, C and E). This outcome is of importance since it tends to indicate that, in some cases, the analytical corrections to be commonly applied to airframe noise experiment might be too excessive, compared to what happens in reality.

[1] On this stage, it is worth mentioning that for CAA-solving a problem as this one with the help of classical 7-point stencil / 6th order standard FD (Finite Difference) schemes, a much denser grid (of more than 200 million cells) would have been required. This is why, here, use was made of the so-called *Intrinsically Optimized Finite Differences* (IOFD) schemes (19), a new class of optimized FD propagation schemes that were recently developed at Onera (Cunha & Redonnet, 2012) and are now implemented in *sAbrinA* solver. One can here recall that such IOFD schemes are of very high accuracy, thanks to an optimization process that is based on a minimization of the scheme's leading-order truncation error (rather than on an optimization of the scheme' spectral properties, such as usually done).

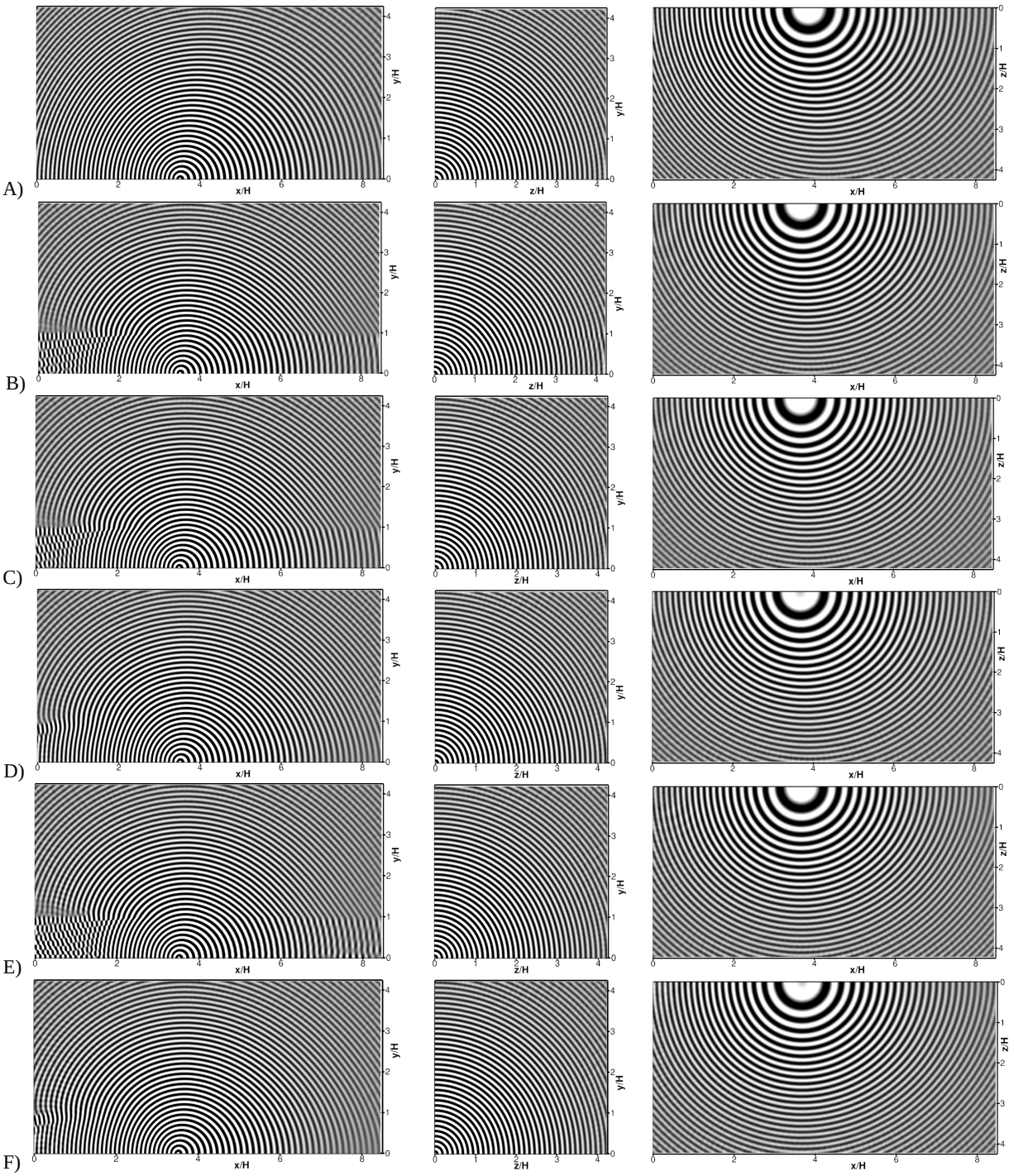

Figure 3 – High frequency (f_8) source radiation, for configurations A to F (from top to bottom, respectively). Instantaneous perturbed pressure within the $z = 0$ (left), $x = 0$ (middle) and $y = 2H$ (right) half-planes

As was said, refraction effects may not only impact the acoustic radiation in terms of amplitude, but also in terms of phase – a thing that may be critical when it comes to apply localization techniques within facility environements. In order to qualitatively highlight that point, Figure 5 displays the acoustic phase counterparts of the RMS maps provided in Figure 4; here again, one can notice how the phase fronts are altered by the shear layer presence, especially when the jet profile is taken as an idealized one (configurations B, C and E).

At this point, one can underline that all the observations made here about the impact of the flow heterogeneities onto the acoustic signature (amplitude reinforcement, phase shifting, etc.) are fully coherent with what can be predicted by the theory and - to some extent - observed in reality.

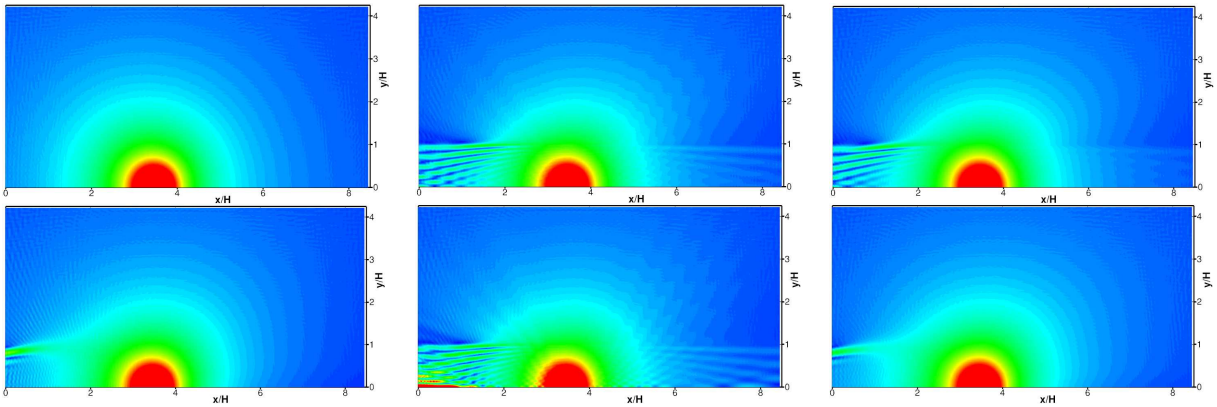

Figure 4 – High frequency (f_8) source radiation, for configurations A to F (clockwise, from top/left). RMS field of the perturbed pressure within the $z = 0$ half-plane

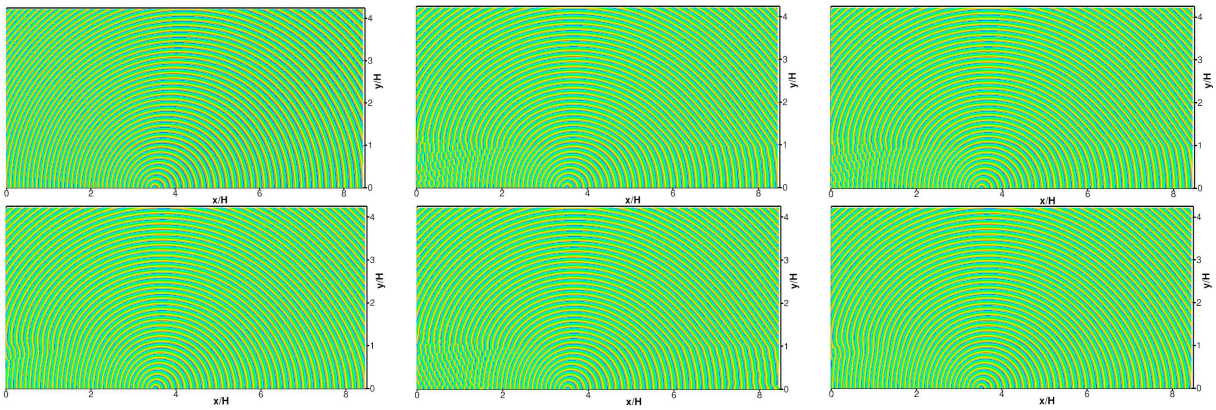

Figure 5 – High frequency (f_8) source radiation, for configurations A to F (clockwise, from top/left). Phase field of the perturbed pressure within the $z = 0$ half-plane

4.2 Refraction Effects by the Various Jet Flows onto the High Frequency Source

In order to characterize more completely how the acoustic energy is diversely impacted by the refraction effects inherited from the various flow profiles, the delta effects between the RMS field obtained for each configuration B to F and the one characterizing the baseline configuration A (uniform flow) are displayed in Figure 6. There, one can appreciate better how each flow profile induces a specific redistribution of the acoustic energy, the latter being strongly reinforced in some parts of the propagation domain (especially in the *xy* plane, but also in the *yz* one for configurations B and C, *i.e.*, when the jet is planar), as well as noticeably attenuated in other areas (see the shadow zones, where deltas exceeds - 2*dB*). Again, it appears that all these reinforcement/attenuation effects are less pronounced when the jet flow is spreading out (configuration D and F) than when its spreading angle is zero (configurations B, C or E). Still by looking at Figure 6, one can also notice how these effects are also driven by parameters such as the shear layer thickness (compare for instance configurations B and C), or jet curvature (compare for instance configurations C and E, or D and F). At the end, it turns out that all these refraction effects onto the acoustic energy are less pronounced when the jet flow is of realistic nature (configuration F) than when it corresponds to more idealized situations (configurations B, C or E, and - to a lesser extent - configuration D). This underlines again how the amplitude corrections that are commonly applied to experimental data (and that are generally derived analytically on the basis of configurations B or E) might be too important, compared to what is really needed in reality.

With the view of illustrating more precisely the refractions effects by the various flows onto the acoustic phase behavior, Figure 7 plots along two y-lines (respectively located on and off the jet axis) the instantaneous perturbed presure field associated with each configuration B to F, comparing it against the one coming from configuration A.

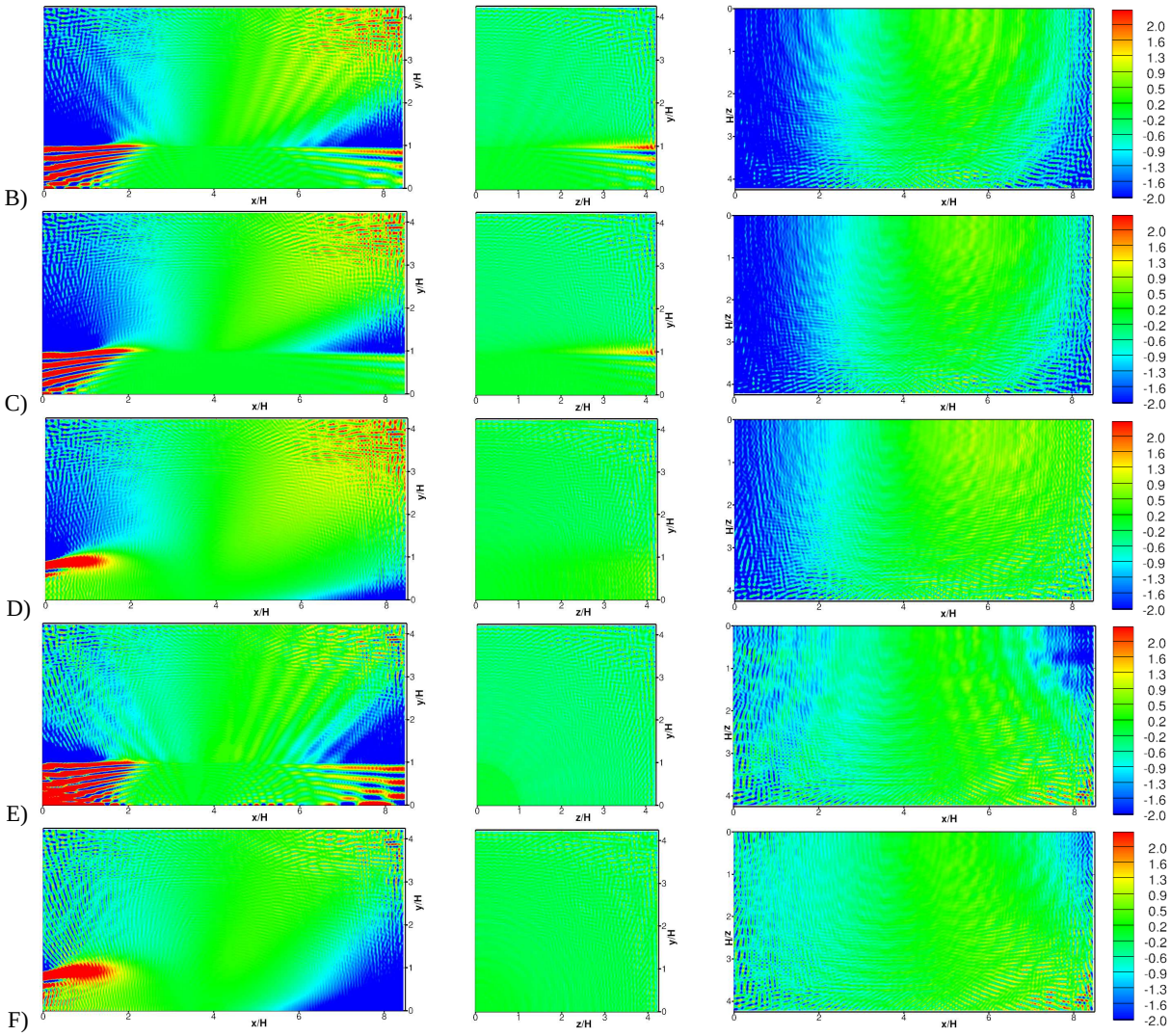

Figure 6 – High frequency (f_8) source radiation. With respect to configuration A, delta (in *dB*) of the RMS field associated with configurations B to F (from top to bottom, respectively), as obtained within the $z = 0$ (left), $x = 0$ (middle) and $y = 2H$ (right) half-planes

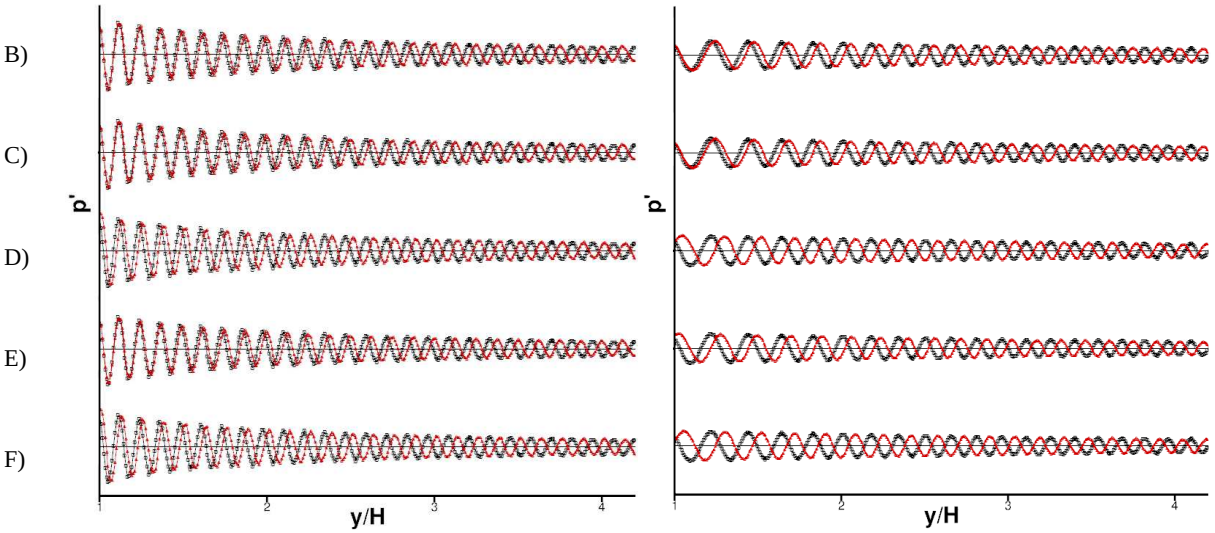

Figure 7 – High frequency (f_8) source radiation. With respect to configuration A (in black), instantaneous perturbed pressure field associated with either configurations B to F (from top to bottom, in red) or configuration A (all curves, in black), as plotted along two *y*-lines, at $x = 3.5H$ and $z = 0$ (left) or $x = 3.5H$ and $z = 2H$ (right)

This Figure highlights well how the jet flow may induce an important phase-shift onto the acoustic waves, with that shift to be more or less pronounced and/or to happen more or less early during the propagation stage, depending on the case. At this stage, one can notice that, contrarily to what was previously observed for the amplitude, here, the acoustic phase appears to be more altered when the jet is spreading out (configurations D and F) than when its spreading angle is zero (configurations B, C and E). In other words, unlike for what happens in terms of acoustic energy amplification/attenuation, the impact that jet flow heterogeneities may have onto the acoustic dispersion may ever be more important when the jet is of realistic nature than when it corresponds to an idealized one.

4.3 Validation of Results against an Analytical Solution

Still regarding the higher frequency (f_8) source, the CAA/PEE simulations associated with configurations A, C, D and F were validated against RT (Ray Tracing) calculations; as an illustration, Figure 8 plots the delta (with respect to configuration A, in *dB*) of the RMS field associated with configurations C, D and F, as delivered by the CAA/PEE and RT calculations within the $z = 0$ half-plane. As one can see, the agreement between both approaches is very satisfactory; indeed, except a few discrepancies (coming from spurious reflections by the free-field boundary condition applied at the periphery of the CAA calculation), both results agree very well, at least above the $y = 0.75\times H$ limit (below which the RT solution is unpredictable).

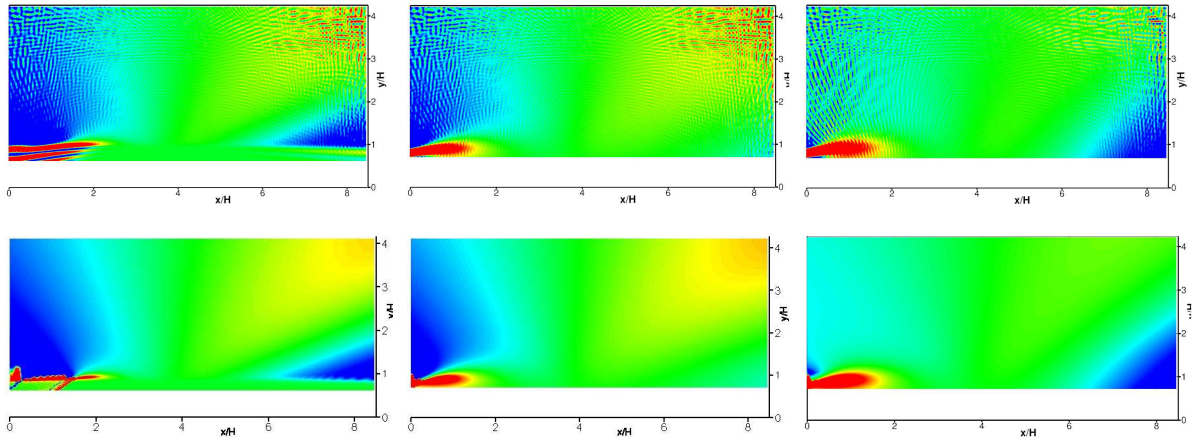

Figure 8 – High frequency (f_8) source radiation. With respect to configuration A, delta (in *dB*) of the RMS field associated with configurations C (left), D (center) and F (right), as delivered by CAA/PEE (top) and RT (bottom) calculations within $z = 0$ half-plane

The same good agreement is also found for what concerns the acoustic phase, as shown in Figure 9, which displays the iso-phase fronts ($\varphi = 0$) obtained for the same configurations C, D and F through both CAA/PEE and RT calculations within the $z = 0$ half-plane; here again, except slight discrepancies occurring in the very upstream part of the shear layers (and coming from the invalidity of the RT solution over this region), both results collapse nicely.

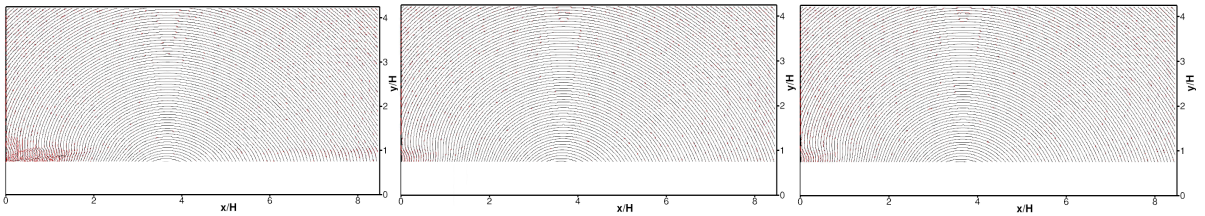

Figure 9 – High frequency (f_8) source radiation. Iso-phase fronts ($\varphi = 0$) field associated with configurations C (left), D (center) and F (right), as delivered by CAA/PEE (black) and RT (red) calculations within $z = 0$ half-plane.

5. CONCLUSIONS

With the view of numerically investigating the refraction effects to be possibly induced by anechoic facility jet flows onto airframe noise experiments, Computational AeroAcoustics (CAA) calculations based

the Perturbed Euler Equations (PEE) were achieved, before they were validated against analytical results coming from a Ray Tracing (RT) technique. The CAA/PEE calculations involved simplistic monopole sources of mid to high frequencies, as well as various background jet mean flows. First analysis of the results focused on the higher frequency source, highlighting how far its radiation may be altered more or less importantly by the various jet flow profiles. This delivered preliminary insights about how refraction effects by jets are primarily driven by specific parameters, such as their shear layers spreading and/or curvature. These outcomes shall be completed in a very near future, thanks to a more complete analysis of all results gathered (e.g., lower frequency cases, etc.).

When completed, the present study shall further aid in the identification of acoustic installation effects that may be important in the type of testing typically done in anechoic facilities (such as NASA's QFF one, but not only). From a more methodological point of view, it shall offer to numerically check the validity and/or accuracy of the analytical corrections (e.g. by Amiet) that are commonly applied to airframe noise experimental data. Finally, coming as a by-product of its validation step, this work shall provide a unique opportunity to compare CAA and ray tracing approaches, in regard to their respective abilities to assess installation effects characterizing realistic facility environments.

ACKNOWLEDGEMENTS

The present study was achieved as part of the International Agreement between NASA and Onera on "*Understanding and Predicting the Source of Nose Landing Gear Noise*". The authors acknowledge Dr. David Lockard, Dr. Mehdi Khorrami and Dr. Meelan Choudhari (all from NASA/LaRC) for their guidance in the definition of this work. The authors also thank other NASA/LaRC personnel, such as Dr. Florence Hutcheson and Mr. Daniel Stead for the detailed information regarding the QFF experimental set up.

REFERENCES

[1]Redonnet, S., Lockard, D. P., Khorrami, M. R. and Choudhari, M. M., "CFD-CAA Coupled Calculations of a Tandem Cylinder Configuration to Assess Facility Installation Effects," *AIAA Paper 2011-2841*, June 2011.

[2]Redonnet, S., "Numerical Assessment of Acoustic Installation Effects Characterizing NASA/LaRC Quiet Flow Facility using Computational AeroAcoustics", *AIAA Paper n° 2014-2628*, June 2014.

[3]Brooks, T. F., and Hodgson, T.H., "Trailing Edge Noise Prediction From Measured Surface Pressures", *Journal of Sound and Vibration*, Vol. **78** n°1, 1981

[4]Jenkins, L. N., Khorrami, M. R., Choudhari, M. M. and McGinley, C. B., "Characterization of Unsteady Flow Structures Around Tandem Cylinders for Component Interaction Studies in Airframe Noise," AIAA Paper *2005-2812*, May 2005.

[5]Hutcheson, F. V. and Brooks, T. F., "Noise Radiation from Single and Multiple Rod Configurations," AIAA Paper *2006-2629*, May 2006.

[6]Humphreys W. M. and Brooks T. F., "Noise Spectra and Directivity for a Scale-Model Landing Gear," AIAA paper 2007-3458, May 2007.

[7]Padois, T., Prax, C. and Valeau V., "Numerical Validation of Shear Flow Corrections for Beamforming Acoustic Source Localization in Open Wind-Tunnels", *Applied Acoustics*, Vol. **74**, 2013.

[8]Amiet R. K., "Correction of open jet wind tunnel measurements for shear layer refraction," *AIAA paper 75-532*, 1975.

[9]Redonnet, S., "Aircraft Noise Prediction via AeroAcoustics Hybrid Methods: Development and Application of Onera Tools over the Last Decade : Some Examples," *Aerospace Lab Journal*, Vol. **7**, June 2014.

[10]Redonnet, S., Manoha, E. and Sagaut, P. "Numerical Simulation of Propagation of Small Perturbations interacting with Flows and Solid Bodies," *AIAA Paper n° 2001-2223*, May 2001.

[11]Redonnet, S., "Simulation de la propagation acoustique en présence d'écoulements quelconques et de structures solides, par résolution numérique des équations d'Euler," *PhD Thesis*, Univ. Bordeaux I, December 2001.

[12]Redonnet, S., Desquesnes, G., Manoha, E. and Parzani, C., "Numerical Study of Acoustic Installation Effects with a CAA Method," *AIAA Journal*, Vol. **48** n°5, May 2010.

[13]Redonnet, S. and Druon, Y., "Computational AeroAcoustics of Realistic Co-Axial Engines," *AIAA Journal*, Vol. **50** n°5, May 2012.

[14]Kirchhoff, G. R., "Zur Theorie der Lichtstrahlen," *Annalen der Physik und Chemie*, Vol. **18**, 1883.
[15]Lighthill, M.J., "On Sound Generated Aerodynamically. I. General theory / II. Turbulence as a source of sound," *Proc. Roy. Soc. London*, Vol. **A 211**, 1952 / Vol. **A 222**, 1954.
[16]Ffowcs-Williams, J. E. and Hawkings, D. L., "Sound Generation by Turbulence and Surfaces in Arbitrary Motion," *Philosophical Transactions of the Royal Society of London* A, Vol. **342**, 1969.
[17]Redonnet, S., "On the Numerical Prediction of Aerodynamic Noise via a Hybrid Approach - Part 1: CFD/CAA Surfacic Coupling Methodology, Revisited for the Prediction of Installed Airframe Noise Problem," *AIAA Paper 2010-3709*, June 2010.
[18]Redonnet, S., Cunha, G., and Ben Khelil, S., "Numerical Simulation of Landing Gear Noise via Weakly Coupled CFD-CAA Calculations," AIAA paper 2013-2068, June 2013.
[19]Cunha, G. and Redonnet, S., "A Novel Optimization Technique for Explicit Finite-Difference Schemes with Application to AeroAcoustics," submitted for publication in *International Journal for Numerical Methods in Fluids*, January 2014.
[20]Redonnet, S., and Bulte, J., "Further Investigation of Acoustic Installation Effects Characterizing NASA/LaRC Quiet Flow Facility using Computational AeroAcoustics," to be presented at 21st AIAA/CEAS AeroAcoustics Conference, Dallas, USA, June 2015.